Accepted Manuscript

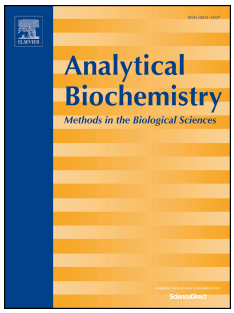

Helix structure of the double-stranded DNA for aptameric biosensing and imaging of cytochrome *c*

Somayeh Pishkar, Azadeh Azadbakh

PII: S0003-2697(17)30401-3

DOI: 10.1016/j.ab.2017.10.016

Reference: YABIO 12821

To appear in: *Analytical Biochemistry*

Received Date: 12 June 2017

Revised Date: 1 October 2017

Accepted Date: 20 October 2017

Please cite this article as: S. Pishkar, A. Azadbakh, Helix structure of the double-stranded DNA for aptameric biosensing and imaging of cytochrome *c*, *Analytical Biochemistry* (2017), doi: 10.1016/j.ab.2017.10.016.

Helix structure of the double-stranded DNA for aptameric biosensing and imaging of cytochrome c

Somayeh Pishkar, Azadeh Azadbakh[a]

[a]*Department of Chemistry, Khorramabad Branch, Islamic Azad University , Khorramabad, Iran.*

Abstract

Here, a method is introduced for construction the aptameric biosensor for biosensing detection of cytochrome C (CYC) based on chain-shape structure of aptasensor by using highly dispersed silver nanoparticles (AgNPs) on acid-oxidized carbon nanotube (CNTs) substrate. The animated capture probe (ssDNA1) and CYC-aptamer (ssDNA2) was immobilized on AgNPs/CNTs surface by covalent amide bonds formed by the carboxyl groups on the nanotubes and the amino groups on the oligonucleotides and hybridization, respectively. In this protocol, the nucleic acids at both ends of the ssDNA1 were sequenced to be complementary (tailor-made ssDNA1). The helix structure of the double-stranded DNA was fabricated by hybridizing ssDNA2 with its complementary sequence (ssDNA1). CYC-aptamer could be forced to dissociate from the sensing interface after CYC triggered structure switching of the aptamer and ssDNA1 thus tend to form a chain-shape structure through the hybridization of the complementary sequences at both its ends. The proposed assay permitted to detect CYC in the linear range of 0.01– 750 nM with a very low limit of detection (LOD) (1.66 pM). In addition, the specificity of this sensing system for the detection of CYC was also demonstrated by using albumin, fructose, myoglobin, and hemoglobin.

Keywords: Aptasensor, Cytochrome C, Helix structure, Silver nanoparticles.

---

*Corresponding author: A. Azadbakht, Tel: +98 6633120399
E-mail: Azadbakht.a@gmail.com

1. Introduction

Cytochrome c (CYC) is a small water-soluble metalloprotein, primarily known as an electron-carrying mitochondrial protein, located in the intermembrane space of mitochondria. It is a polypeptide chain consisting of 104 amino acid constituent, covalently attached to one heme-group [1, 2]. The transition of this mitochondrial redox chromo-protein between the ferrous and ferric states within the cell plays an indispensable role in the oxidative phosphorylation process [3, 4]. Normally, in the presence of CYC on the mitochondrial membranes, it acts as an electron carrier in the mitochondrial inter-membrane space between CYC-reductase and CYC-oxidase via the redox reaction of its iron content. Whereas, in the absence of CYC, owning to electron exchange chain blockage, the significant decline of adenosine triphosphate content is occurred. This phenomena lead to incomplete oxidation process and exceeding producing of the superoxide radical [5].

Taking the electron transfer reactions of CYC into consideration, it is served in various electrochemical sensors as redox mediator for electrochemical recognition and electrocatalysis of verity number of compound including nitric oxide [6], nitrite [7], hydrogen peroxide [8, 9], superoxide radical [10] and so on. For these reasons, there is an urgent need in the development of simple and reliable sensors to evaluate its concentration. So, several experimental technique have been developed for CYC quantification. These include fluorometry [11] electrophoresis [12], chemiluminescence [13], flow cytometry [14], high performance liquid chromatography (HPLC) [15], and electrochemistry [16, 17]. Although most of the instrument-based methods have some advantages like rapid analysis, they are restricted with expensive and complicated instruments, extensive pretreatment of the sample, and requiring skillful and experienced technician. Also, taking the interaction of electrochemical biosensors with other small proteins into account, the electrochemical devices suffer from lack of selectivity for CYC detection [18]. Alternatively, aptameric electrochemical biosensors have been emerged as a promising approach in order to overcome these limitations.

Recently, the use of oligonucleic acid (either DNA or RNA, known as aptamer) or peptide molecules with high binding capabilities has attracted promising attention. The process through which these molecules are isolated in vitro is called selective evolution of ligands by exponential enrichment (SELEX) [19]. On account of their remarkable characteristics consisting easy preparation, facile modification, reusability, thermal stability, biological compatibility, and general availability for almost any given protein, aptamer-based sensor have been widely served for environmental monitoring [20] and medical examination [21].

In this study, our research group work on construction of an electrochemical aptamer based assay for CYC recognition by employing amine-capped DNA sequence (ssDNA1) as a capture probe, CYC specific aptamer (ssDNA2) as a detection probe, and silver nanoparticles (AgNPs) decorated on acid-oxidized carbon nanotube (CNT-COOH) as a sensing substrate. Firstly, AgNPs/CNT-COOH was placed at the surface of glassy carbon (GC) electrode. Next, ssDNA1 and CYC specific aptamer were immobilized at the surface of modified electrode through the covalent amide bonds formation and hybridization, respectively. Displacement of surface-bound aptamer to form a complex with target molecule in solution leads to a increase in the electron-transfer resistance. Signaling in this protocol arises from changes in electron transfer efficiency upon target-induced changes in the conformation of the aptamer probe. These changes were monitored electrochemically by using electrochemical impedance spectroscopy (EIS) technique.

2. Experimental

2.1. Chemicals

Multiwall carbon nanotubes with purity 95% (10–20 nm diameters) and 1 µm length were obtained from Nanolab (Brighton, MA). Silver nitrate ($AgNO_3$, 99.7%), potassium chloride (KCl), potassium nitrate (KNO_3), potassium ferricyanide ($K_3Fe(CN)_6$), and potassium ferrocyanide ($K_4Fe(CN)_6$) were purchased from Merck (Germany) and Fluka. N-hydroxysuccinimide (NHS), 1-Ethyl- 3-(3-dimethylaminopropyl) carbodiimide hydrochloride (EDC), albumin, hemoglobin, fructose, and myoglobin were commercially available from Sigma-Aldrich (St. Louis, USA) and used without further purification. All of the aqueous solutions were prepared with double-distilled water. Oligonucleotides designed according to the literature [22] in the present manuscript were synthesized and purified by Bioneer (South Korea). Sequences of oligonucleotides were shown as following, the CYC-binding aptamer (5'- CCG TGT CTG GGG CCG ACC GGC GCA TTG GGT ACG TTG TTG C-3') and its complementary oligonucleotide modified with $–NH_2$ at the 3′ end (3'-NH_2-$(CH_2)_6$GGC ACA GAC CCC TGC C-5'). Phosphate buffered solution (PBS) was employed as working buffer throughout the experiment with constitute of 0.1M Na_2HPO_4, 0.1 M KH_2PO_4 and 0.5 M NaCl. All experiments were performed at ambient temperature of 25 ±1 ◦C.

2.2. Apparatus

Cyclic voltammetry (CV), electrochemical impedance spectroscopy (EIS), and differential pulse voltammetry (DPV) measurements were performed by using a computer controlled Autolab potentiostat/galvanostat (PGSTAT204, Eco-Chemie, The Netherlands).

The data were analyzed by NOVA 1.8 and Frequency Response Analyzer (FRA) software. Also, a personal computer for data storage and processing was used. A three-electrode electrochemical system was employed with an saturated Ag/AgCl electrode (KCl, 3 M) as the reference electrode, a platinum wire as counter electrode, and a modified and unmodified disk glassy carbon (GC) electrode as working electrode. JENWAY pH meter (model 3345) was also applied for pH measurements. To obtain MilliQ water was supplied into MilliQ machine which purified deionized water even further.

2.3. CV, DPV, and EIS measurements

CV technique was performed at room temperature in 10 mL of 0.1 M PBS containing 5.0 mM $K_3[Fe(CN)_6]/K_4[Fe(CN)_6]$ (1:1) in the voltage range of -0.8 V to 1.0 V at a scan rate of 50 mVs^{-1}. Furthermore, DPV measurement was recorded in 10 mL of 0.1 M PBS containing 5.0 mM $K_3[Fe(CN)_6]/K_4[Fe(CN)_6]$ (1:1) at room temperature with a modulation amplitude of 0.05 V, a pulse width of 0.05 s, and sample width of 0.0167 s.

Impedance analysis was carried out at an applied potential of 0.2 V (vs. Ag/AgCl reference electrode) obtained from the redox potential of $K_3[Fe(CN)_6]/K_4[Fe(CN)_6]$ by CV, with a frequency range between 0.1 Hz and 100 kHz, an signal amplitude of 5 mV and a sampling rate of 10 points per decade above 66 Hz and 5 points per decade at the lower range. All EIS data were obtained in the solution containing 0.1 M PBS, 5.0 mM $K_3Fe(CN)_6$ and $K_4Fe(CN)_6$, used as a redox marker. The morphology of nanocomposite, size and distribution of nanoparticles were investigated using the scanning electron microscopy microscope (SEM, X-30 Philips instrument). Moreover, the energy-dispersive X-ray (EDS) and wavelength-dispersive X-ray (WDX) spectroscopy were employed by a Vega-Tescan electron microscope.

2.4. Electrochemical sensor preparation

Prior to modification, the glassy carbon surface was successively polished with 0.05 mm α-Al_2O_3 power slurries on a polishing cloth until a shiny mirror- like surface was achieved. In the next step, the resultant electrode was ultrasonically cleaned in 1:1 acetone: double-distilled water for 10 min and dried at room temperature in a vacuum oven for 1 h. Then, 1 mg of CNTs was dispersed in 1 mL DMF and ultrasonicated for 30 min to form a homogeneous black suspension. Next, 10 μL of suspension dispersion was carefully pipetted onto the surface of the GC electrode. AgNPs/CNTs/GC electrode was fabricated by electrochemical potentiostatic deposition of AgNPs, according to a one-step procedure reported in the literature [23]. Briefly, the CNTs/GC electrode was immersed in a solution

containing 5×10^{-3} M $AgNO_3$ and 0.1 M KNO_3 under a constant potential of -0.40 V to the working electrode for 10 s. AgNPs can facilitate more efficient electron transfer e.g. harboring more active sites on their surface [24-26]. Also, it was served in order to immobilize animated capture probe (ssDNA1) on the surface of sensing interface by chemisorption between silver nanoparticles and amino groups of ssDNA1. In the next step, 10 μL ssDNA1 solutions prepared in PBS containing EDC and NHS was placed on the electrode surface and the electrode was kept for 2 h at 4 °C. During this process, the 3′-amino group of the probe oligonucleotides was covalently bonded to the carboxyl group of carbon nanotubes. In addition, the chemisorption of aptamer on the surface of the AgNPs was occurred as a result of interaction between amino group of oligonucleotides and AgNPs (the electrode denoted ssDNA1/AgNPs/CNTs/GC electrode). The order of nucleic acid in the capture probe was rationally sequenced as 3'-NH_2-$(CH_2)_6$GGC ACA GAC CCC TGC C-5' by introducing four bases (i.e., GGCA) at the 3′ end, which are complementary to the bases at the 5′ end (i.e., TGCC). Then the modified electrode was thoroughly rinsed with water to remove the weakly adsorbed ssDNA1. The last step consisted of aptamer immobilization onto the electrode surface. For this goal, 10 μL of aptamer solution in MilliQ water at the desired concentration was dropped at the surface of ssDNA1/AgNPs/CNTs/GC electrode overnight at 4 °C which results in a half-duplex DNA structure formation at the surface of sensing platform (the electrode denoted aptamer/AgNPs/CNTs/GC electrode). This step was followed by two washing steps using PBS buffer solution so as to remove any unabsorbed CYC-aptamer.

3. Results and discussion

3.1. Sensing strategy of the aptasensor

The electrochemical sensing surface for CYC recognition was fabricated by functionalizing the AgNPs/CNTs/GC electrode with half-duplex hybridized by animated part complementary DNA strand (ssDNA1) and CYC-binding aptamer strand (ssDNA1). The aptameric biosensing of CYC was carried out based on the CYC-binding induced conformational change of ssDNA1 oligonucleotides, from a half-duplex helix to a single-stranded oligonucleotide and finally to a chain shape structure. When the sensing interface was exposed with CYC solution, the interaction between CYC and its aptamer probe resulted in the displacement of aptamer strand from the sensing interface while capture probe was still bound to electrode surface. Due to the existence of four complementary sequences at both ends of the capture probe, the ssDNA1 folded and chain shape structure was formed at the surface of modified electrode. Based on the procedure reported in the literature, Mg^{2+} could

induce the structural conversion of ssDNA1 with complementary nucleic acids at both ends from a single stranded oligonucleotide into a chain shape structure [27]; as a consequence, CYC monitoring was performed in the presence of $MgCl_2$ to induce the formation of the chain shape structure of ssDNA1 assembled onto the electrode surface. The preparation of different steps of sensing interface and the CYC detection are shown in Fig. 1. In the absence of CYC, the half-duplex helix structure of oligonucleotides on the surface of sensing substrate was entire. Thus, it was reasonable to observe small charge transfer resistance (R_{ct}) for modified electrode. When the sensing platform was immersed into an CYC solution, half-duplex DNA was transited to chain shape DNA, which block the electron exchange of $[Fe(CN)_6]^{3-/4-}$, led to increased electrochemical EIS response.

3.2. Characterization and optimization of sensing interface

Scanning electron microscopy (SEM) was conducted before and after CNTs casting and AgNPs electrodeposition to trace the effects of modification process on the morphology and structure of the bare GC electrode. The surface morphology of bare GC electrode (A), CNTs/GC (B), AgNPs/GC (C), and AgNPs/CNTs/GC (D) modified electrodes are shown in Fig. 2. As could be seen, the CNTs casting significantly change the morphology of the bare GC surface. In fact, the CNTs produce a net-like structure, offering a good accessible surface area (Fig 2B). The AgNPs electrodeposition results in formation of well dispersed nanoparticles structure (Fig 2C). The AgNPs/CNTs/GC modified electrode consists of both nanowire and nanoparticles which the spaghetti- like structures is associated with CNTs and globular structures indicated with arrow are related to AgNPs (Fig 2D). The SEM imaging with the corresponding energy-dispersive X-ray (EDS) analyses of nanocomposite (Fig. 3A) suggests that the species supported on the CNTs surfaces is Ag element. Also, EDS spectrum proves the existence of C, and O in the nanocomposite, indicating that the composite includes both CNTs and AgNPs. To further acknowledge the presence of C, O, and Ag elements, the WDX evidence were used and the distribution of C, O, and Ag are shown in Fig. 3B-3D.

3.3. Optimum concentration of CYC-aptamer

In order to improve the performance of the aptasensor, the experimental aptamer concentration on the sensing interface was optimized. For this goal, different concentrations of the aptamer (0.5, 1.0, 2.5, 5.0 μM) were immobilized on the electrode surface and the interfacial resistance value of all aptasensors were recorded as a control response (Fig. 4, curves a in all plot). In the next step, the R_{ct} response of all aptasensor after incubation in the solution containing constant amount of CYC was monitored (Fig. 4, curves b in all plot) and

the interfacial resistance value change (ΔR_{ct}) of aptasensors in the absence and presence of CYC was assessed. As shown in Fig. 4, the ΔR_{ct} value was increased with prolonging concentration of CYC-aptamer from 0.5 -2.5 μM (saturation value) and then decreased. Based on the results, it was obviously concluded that the electrode sensitivity was strictly dependent on the aptamer concentration. The more concentrated the aptamer concentration are, the larger changes are in the ΔR_{ct} value up to 2.5 μM aptamer content. The poorer sensitivity of aptasensor at higher concentrations of aptamer can be related to the inactivation of some aptamers, reducing the response as fewer of the probes undergo binding with target proteins. At higher concentration of aptamer, some unfavorable event such as steric/conformational restrictions and undesirable interactions between neighboring aptamers (cross hybridization) might happened which caused the decrease of sensitivity of sensing interface. Therefore, 2.5 μM was chosen as optimized aptamer concentration for subsequent experiments.

3.4. Optimum incubation time of the proposed aptasensor

The dependence of DPV current signal intensity and also EIS charge transfer resistance value of aptasensor on incubation time were investigated and the results are shown in Fig. 5. Fig. 5A represented the DPV current response of aptamer/AgNPs/CNTs/GC before (solid line) and after (dashed line) incubation of aptameric biosensor with 100 nM CYC with increasing incubation time, recorded in the solution containing 5.0 mM $[Fe(CN)_6]^{3-/4-}$ and 0.1 M PBS. Also, the change of R_{ct} value of aptasensor in the absence (solid line) and presence (dashed line) of 100 nM CYC with various incubation times were recorded and the signals are presented in Fig.5B. According to results, the maximum ΔR_{ct} and Δ_{ip} value were recorded for 30 min incubation time and after 40, and 50 min the change of aptasensor response tended to level off, confirming the complete of the cleavage procedure. Therefore, 30 min was chosen as optimum incubation time for subsequent experiment.

3.5. Electrochemical behavior of aptasensor

In order to follow the barrier changes of the electrode surface before and after each immobilization binding step, impedance measurements and cyclic voltammetry were applied. Comparison between the CV of $[Fe(CN)_6]^{3-/4-}$ at the surface of GC (curve a), AgNPs/CNTs/GC (curve b), ssDNA1/AgNPs/CNTs/GC (curve c), aptamer/AgNPs/CNTs/GC (curve d) and CYC/aptamer/AgNPs/CNTs/GC (curve e) are shown in Fig. 6. According to Fig. 6, maximum redox peak current at the surface of AgNPs/CNT/GC electrode was observed, which could be associated with enhancement of the

conductivity and improving the effective surface area of the electrode surface. As it is obvious from our data, after immobilization of ssDNA1 at the surface of AgNPs/CNTs/GC electrode, a smaller anodic peak current intensity was recorded, confirming that the ssDNA1 can relatively hinder the electron transfer of redox probe to the aptasensor surface. Due to the negative surface charges of ssDNA2 and limited diffusion of $[Fe(CN)_6]^{3-/4-}$ toward electrode surface , the current response of aptamer/AgNPs/CNTs/GC after immobilization of ssDNA2 decreased. After CYC incubation, the CV current response further decreased due to blockage the electron transfer of redox probe as a result of chain shape structure formation on the electrode surface.

EIS could reflect the impedance changes of the electrode surface during the modification process. Faradaic impedance spectra were recorded as a Nyquist plot and data were adjusted to a Randles equivalent circuit. Thus, the electron transfer capability of these different sensing devices was recorded by electrochemical impedance technique. Fig. 7 shows the Nyquist plot of GC (curve a), AgNPs/CNTs/GC (curve b), ssDNA1/AgNPs/CNTs/GC (curve c), aptamer/AgNPs/CNTs/GC (curve d) and CYC/aptamer/AgNPs/CNTs/GC (curve e) modified electrodes recorded in the solution containing 0.1 M PBS and 5.0 mM $[Fe(CN)_6]^{3-/4-}$ at open circuit potential with the frequency varied from 0.1 Hz to 10,000 Hz. As expected, the minimum charge transfer resistance was obtained for AgNPs/CNTs/GC, proving the results obtained by CV technique. After ssDNA1 and ssDNA2 attachments, R_{ct} increased due to the physical coverage by the oligonucleotides and the repulsive electrostatic interaction between negatively charged phosphate backbone of the DNA and $[Fe(CN)_6]^{3-/4-}$. Incubation of CYC-aptasensor in solution containing the CYC, caused the dramatically increasing in the R_{ct} value (curve e), suggesting an effective barrier to the electron transfer of redox probe in solution. The EIS data corroborated the preceding results obtained by CV, all confirmed that the sensing interface has been achieved successfully.

3.6. Analytical performance of the aptasensors

The quantitative behavior of the fabricated biosensors was investigated by incubating the aptamer/AgNPs/CNTs/GC sensor in the solutions of different concentrations of CYC and analyzing the change of electrochemical charge transfer resistance intensity of the modified electrode in the solution containing $[Fe(CN)_6]^{3-/4-}$ as redox probe. As shown in Fig. 8A, the EIS charge transfer resistance value increased with increasing concentration of CYC and reached to a maximum R_{ct} value for CYC concentration up to 750 nM. The dose response signal revealed a strong linear dependence of R_{ct} value on the CYC concentration in the range

from 0.01 to 750 nM (Fig. 8B) with the correlation coefficient of 0.9892. The limit of detection (LOD) was calculated to be 1.66 pM from three times standard deviation corresponding to the blank sample detection. As shown in Table 1, this proposed assay offered prominent analytical performance compared with other methods and techniques in terms of the detection limit and linear concentration range, as listed in Table 1 [28 - 35].

3.7. Selectivity, stability and reproducibility of aptasensor

Under the optimal conditions, the selectivity, stability and reproducibility of proposed aptasensor were assessed. As shown in Fig. 9, the selectivity of electrochemical assay was estimated by both DPV and EIS techniques. The control experiments were carried out by incubating the aptasensor with 100 μM of several analog compound including albumin, fructose, myoglobin, and hemoglobin. Afterwards, the EIS and DPV signal were recorded in the presence of $[Fe(CN)_6]^{3-/4-}$ redox couple. The selectivity of the aptasensor was evaluated by tracing the R_{ct} and anodic peak current (I_p) changes when the sensor treated with other species instead of CYC. When the control interferents were incubated with the aptamer/AgNPs/CNTs/GC, the change of R_{ct} value for EIS and I_p for DPV signal were negligible, confirming that these related compounds can hardly specifically combined with the aptasensor. Conversely, incubation of aptasensor in the solution containing CYC even at 1000-fold lower concentrations than that of interfering compounds led to the significant change in charge transfer resistance and anodic peak current of $[Fe(CN)_6]^{3-/4-}$. These results indicated that the fabricated aptasensor had high binding affinity and selectivity to the CYC.

Also, the stability of the aptasensor is considered as a key factor in applied applications, which was investigated by rinsing, drying, and storing the sensor in 4°C in a refrigerator. Based on the results, after 2 weeks, just 4.5 % decrease was observed for the CYC response at the same concentration, suggesting good stability of voltammetric signal. Also, 7.1 % reduction for the anodic peak current of CYC after 4 weeks was found, stating good stability of the sensor. The reproducibility of the fabricated aptasensor was examined by expressing the relative standard deviation (RSD) of the response of five modified electrodes freshly prepared in the presence of 100 nM CYC. According to our data, the RSD of the prepared aptasensors were found to be 4.4%, indicating that the aptasensor fabrication process was reproducible.

3.8. Real sample analysis

The capability of the aptasensor for clinical CYC diagnostic was examined by determination of CYC content in human serum sample. Human serum sample was prepared

as following procedure. First, 2 mL methanol was added to 1.5 mL of serum sample. Then, the serum sample was vortexed for 2 min and the precipitated proteins were separated by centrifugation for 3 min at 6000 rpm. Finally, the transparent supernatant solution was filtered through 0.45 μm milli-pore filter. The obtained protein-free human serum sample was then employed for CYC analysis. For this goal, three human serum samples were spiked with various concentrations of CYC and CYC content were tested using five independently sensors. As shown in Table 2, the recoveries of spiked samples were between 97.6% and 105% when using this method, which showed a satisfactory result and confirmed that the aptamer/AgNPs/CNTs/GC represented a good capability for the analysis of pharmaceutical and biological samples.

4. Conclusion

An ultrasensitive label-free electrochemical aptasensor for CYC recognition was introduced with silver nanoparticles (AgNPs) on acid-oxidized carbon nanotube (CNTs) substrate, amine-capped DNA sequence (ssDNA1) as a capture probe, CYC-aptamer (ssDNA2) as a detection probe, and $[Fe(CN)_6]^{3-/4-}$as redox probe. The sequences of nucleic acid at both ends of the ssDNA1 are engineered to be complementary. The higher binding constant of the aptamers with CYC than that with ssDNA1 led to release of the aptamer from its complementary strand into solution and destruction the Watson-Crick helix structure of the double-stranded DNA assembled onto the electrodes surface. Mg^{2+} could stimulate the formation of the chain-shape structure of ssDNA1 in the next step, leading to the low access of $[Fe(CN)_6]^{3-/4-}$ to the surface of modified electrode, and decreased electrochemical signal. The detection limit for determination of CYC was found to be as low as 1.66 pM at concentration range up to 750 nM. The designed aptasensor can be served successfully for CYC diagnostic in biological samples and it can provide an evaluable tool for clinical medicine diagnostic.

Acknowledgements

The authors gratefully acknowledge the support of this work by the Khorramabad Branch, Islamic Azad University for financial support.

References

[1] A. L. Raphael, HB. Gray, Semisynthesis of axial-ligand (position 80) mutants of cytochrome c, J. Am. Chem. Soc. 113 (1991)1038-1040.

[2] D. R Green, G. Kroemer, The pathophysiology of mitochondrial cell death, Science, 305 (2004) 626-629.

[3] M. Huttemann, P. Pecina, M. Rainbolt, T. H. Sanderson, V. E. Kagan, L. Samavati, The multiple functions of cytochrome c and their regulation in life and death decisions of the mammalian cell: from respiration to apoptosis, Mitochondrion, 11(2011) 369-381.

[4]Y. P. Ow, D.R. Green, Z. Hao, T.W. Mak, Cytochrome c: functions beyond respiration, Nat. Rev. Mol. Cell. Biol. 9 (2008) 532-542.

[5] S. G. Sivakolundu, P. A. Mabrouk, Structure-function relationship of reduced cytochrome c probed by complete solution structure determination in 30% acetonitrile/water solution, J. Biol. Inorg. Chem 8 (2003)527–539.

[6] Y. C. Liu, J. Zhao, W. L. Wu, Z. S. Yang, Direct electrochemical behavior of cytochrome c on DNA modified glassy carbon electrode and its application to nitric oxide biosensor, Electrochim. Acta 52 (2007) 4848–4852.

[7] M. Eguílaz, L. Agüí, P. Yá˜nez-Sede˜no, J.M. Pingarrón, A biosensor based on cytochrome c immobilization on a poly-3-methylthiophene/multi-walled carbon nanotubes hybrid-modified electrode. Application to the electrochemical determination of nitrite, J. Electroanal. Chem. 644 (2010) 30-35.

[8] S. Lata, B. Batra, N. Karwasra, C. S. Pundir, An amperometric H_2O_2 biosensor based on cytochrome c immobilized onto nickel oxidenanoparticles/carboxylated multiwalled carbon nanotubes/polyanilinemodified gold electrode, Process. Biochem. 47 (2012) 992–998.

[9] A. K. Yagati, T. Lee, J. Min, J. W. Choi, Electrochemical performance of gold nanoparticle-cytochrome c hybrid interface for H_2O_2 detection, Colloids Surf. B, 92 (2012) 161–167.

[10] P. Rahimi, H. Ghourchian, H. A. Rafiee-Pour, Superoxide radical biosensor based on a nanocomposite containing cytochrome c, Analyst, 136 (2011)3803–3808.

[11] Y. Shen, X. F. Yang, Y. Wu, C. Li, Sensitive spectrofluorimetric determination of cytochrome c with spirocyclic rhodamine B hydrazide in micellar medium, J. Fluoresc. 18 (2008)163-168.

[12] S. N. Tan, L. Hua, Amperometric detection of cytochrome c by capillary electrophoresis at a sol-gel carbon composite electrode, Anal. Chim. Acta, 450 (2001) 263-267.

[13] X. Li, H. Liu, X. He, Z. Song, Determination of Cytochrome *c* in Human Serum and Pharmaceutical Injections Using Flow Injection Chemiluminescence, Appl. Biochem. Biotechnol. 160 (2010)1065-1073.

[14] C. B. Campos, B. A. Paim, R. G. Cosso, R. F. Castilho, H. Rottenberg, A. E. Vercesi, Method for monitoring of mitochondrial cytochrome c release during cell death: immune detection of cytochrome c by flow cytometry after selective permeabilization of the plasma membrane, Cytom. Part A, 69 (2006)515–523.

[15] E. D. Crouser, M. E. Gadd, M. W. Julian, J. E. Huff, K. M. Broekemeier, K. A. Robbins, D. R. Pfeiffer, Quantitation of cytochromec release from rat liver mitochondria, Anal. Biochem. 317 (2003) 67-75.

[16] M. Pandiaraj, T. Madasamy, P. N. Gollavilli, M. Balamurugan, S. Kotamraju, V. K. Rao, K. Bhargava, C. Karunakaran, Nanomaterial-based electrochemical biosensors for cytochrome *c* using cytochrome *c* reductase, Bioelectrochemistry, 91 (2013) 1-7.

[17] D. Luo, J. Huang, Determination of Cytochrome c and Other Heme Proteins Using the Reduction Wave of Mercury Protoporphyrin IX Groups Generated by a Hydroxylamine Induced Replacement Reaction, J. Anal. Chem. 81 (2009) 2032-2036.

[18] Q. Wen, X. Zhang, J. Cai, P. H. Yang, A novel strategy for real-time and *in situ* detection of cytochrome c and caspase-9 in Hela cells during apoptosis, Analyst, 139 (2014) 2499-2506.

[19] R. Stoltenburg, C. Reinemann, B. Strehlitz, FluMag-SELEX as an advantageous method for DNA aptamer selection, Anal. Bioanal. Chem. 383 (2005) 83–91.

[20] S. Li, C. Liu, G. Yin, Q. Zhang, J. Luo , N. Wu, Aptamer-molecularly imprinted sensor base on electrogenerated chemiluminescence energy transfer for detection of lincomycin, Biosens. Bioelectron. 91 (2017) 687–69.

[21] K. Abnous, N. M. Danesh, M. Alibolandi, M. Ramezani, S. M. Taghdisi, A. S. Emrani, A novel electrochemical aptasensor for ultrasensitive detection of fluoroquinolones based on single-stranded DNA-binding protein, Sens. Actuat.: B. Chem. 240 (2017)100–106.

[22] I. P. M. Lau, E. K. S. Ngan, J. F. C. Loo, Y. K. Suen, H. P. Ho, S. K. Kong, Aptamer-basedbio-barcode assay for the detection of cytochrome-c released from apoptoticcells, Biochem. Biophys. Res. Commun. 395 (2010) 560–564.

[23] L. Guadagnini, D. Tonelli, Carbon electrodes unmodified and decorated with silver nanoparticles for the determination of nitrite, nitrate and iodate, Sens. Actuat. B, 188 (2013) 806-814.

[24] L. Yu, Y. Shi, Z. Zhao, H. Yin, Y. Wei, J. Liu, W. Kang, T. Jiang, A. Wang, Ultra small silver nanoparticles supported on silica and their catalytic performances forcarbon monoxide oxidation, Catal. Commun. 12(2011) 616-620.

[25] G. L. Wang, X. Y. Zhu, H. J. Jiao, Y. M. Dong, X. M. Wu, Z. J. Li, Oxidative etching-aggregation of silver nanoparticles by melamine and electron acceptors: aninnovative route toward ultrasensitive and versatile functional colorimetricsensors, Anal. Chim. Acta, 747(2012) 92-98.

[26] A, Valipour, M. Roushani, Using silver nanoparticle and thiol graphene quantum dots nanocomposite as a substratum to load antibody for detection of hepatitis C virus core antigen: Electrochemical oxidation of riboflavin was used as redox probe, Biosens. Bioelectron. 15 (2017) 946-951.

[27] Y. Lu, X. Li, L. Zhang, P. Yu, L. Su, L. Mao, Aptamer-based electrochemical sensors with aptamer-complementary DNA oligonucleotides as probe, Anal. Chem. 80 (2008) 1883-1890.

[28] Y. P. Dong, Y. Peng, J. Wang, C. M. Wang, Determination of cytochrome c based on its enhancing effect on the electrogenerated chemiluminescence of carbon quantum dots, Microchim. Acta, in press

[29] L. Ma, F. Liu, Z. Lei, Z. Wang, A novel upconversion@polydopamine core@shell nanoparticle based aptameric biosensor for biosensing and imaging of cytochrome c inside living cells, Biosens. Bioelectron. 87 (2017) 638‑645.

[30] X. H. Yin, J. Cai, H. Y. Feng, Z. M. Wu, J. M. Zou, Q. Y. Cai, A novel VS_2 nanosheet-based biosensor for rapid fluorescence detection of cytochrome c, New J. Chem. 39(2015)1892–1898.

[31] F. Salehnia, M. Hosseini, M. R. Ganjali, A fluorometric aptamer based assay for cytochrome C using fluorescent graphitic carbon nitride nanosheets, Microchim. Acta, in press

[32] C. Ocana, E. Arcay, M. del Valle, Label-free impedimetric aptasensor based on epoxy-graphiteelectrode for the recognition of cytochrome, Sens. Actuat. B, 191 (2014) 860– 865.

[33] X.W. Hu, C. J. Mao, J.M. Song, H. L. Niu, S.Y. Zhang, H.P. Huang, Fabrication of GO/PANi/CdSe nanocomposites for sensitive electrochemiluminescence biosensor. Biosens. Bioelectron. 41(2013) 372–378.

[34] C. Ocana, S. Lukic, M. del Valle, Aptamer-antibody sandwich assay for cytochrome c employing an MWCNT platform and electrochemical impedance, Microchim. Acta, (2015) 182:2045‑2053.

[35] F.C. Loo, S.P. Ng, C.M. L. Wu, S. K. Kong, An aptasensor using DNA aptamer and white light common-path SPR spectral interferometry to detect cytochrome-c for anti-cancer drug screening. Sens. Actuat. B, 198(2014) 416-423.

Figure caption

Fig. 1 Schematic representation of different steps of aptasensor fabrication.

Fig. 2 Typical SEM images of bare GC (A), CNTs/GC (B), AgNPs/GC (C), and AgNPs/CNTs/GC (D) modified electrodes.

Fig. 3 (A) EDS spectrum of the AgNPs/CNTs/GC nanocomposite . WDX analysis for (B) C, (C) O, and (D) Ag elements.

Fig. 4 Nyquist plot of aptamer/AgNPs/CNTs/GC electrode after immobilization increasing concentration of CYC-aptamer at the surface of electrode in the absence (curve a) and presence (curve b) of 100 nM CYC, recorded in the solution containing 5.0 mM $[Fe(CN)_6]^{3-/4-}$ and 0.1M PBS.

Fig. 5 (A) DPV current results and (B) Nyquist plot of aptamer/AgNPs/CNTs/GC electrode after increasing incubation time in the absence (solid line) and presence (dashed line) of 100 nM CYC, recorded in the solution containing 5.0 mM $[Fe(CN)_6]^{3-/4-}$ and 0.1 M PBS.

Fig. 6 CV plots for of GC (curve a), AgNPs/CNTs/GC (curve b), ssDNA1/AgNPs/CNTs/GC (curve c), aptamer/AgNPs/CNTs/GC (curve d) and CYC/aptamer/AgNPs/CNTs/GC (curve e) electrodes recorded the solution containing 5.0 mM $[Fe(CN)_6]^{3-/4-}$ and 0.1M PBS.

Fig. 7 Nyquist plots for of GC (curve a), AgNPs/CNTs/GC (curve b), ssDNA1/AgNPs/CNTs/GC (curve c), aptamer/AgNPs/CNTs/GC (curve d) and CYC/aptamer/AgNPs/CNTs/GC (curve e) electrodes recorded the solution containing 5.0 mM $[Fe(CN)_6]^{3-/4-}$ and 0.1M PBS.

Fig. 8 (A) Nyquist plots for prepared aptasensor recorded in solution containing 5.0 mM $[Fe(CN)_6]^{3-/4-}$ and 0.1 M PBS after incubation with different concentration of CYC: 0.01, 0.1, 0.5, 1, 5, 30, 60, 90, 250, 500, and 750 nM. (B) Plots of R_{ct} vs. CYC concentrations.

Fig. 9 (A) Nyquist plot and (A) DPV current results of the proposed aptasensor before (solid line) and after (dashed line) being incubated with 100 μM albumin, fructose, myoglobin, hemoglobin and 100 nM CYC in the solution containing 5.0 mM $[Fe(CN)_6]^{3-/4-}$ and 0.1M PBS.

Table 1 Comparison between analytical performance of this method and other reported techniques for detection of CYC.

Electrode and sensor	Technique	LOD	Linear range	Refs.
Carbon quantum dots /glassy carbon electrode	Electrogenerated chemiluminescence	0.20 nM.	1.00 nM to 10.0 μM	[28]
Polydopamine core@shell nanoparticle	Fluorescence	20.0 nM	50.0 nM to 10.0 μM	[29]
VS_2 nanosheet	Fluorescence	0.50 nM	0.75 nM to 50.0 μM	[30]
Graphitic carbon nitride nanosheets	Fluorescence	2.60 nM.	16.0 nM to 140 nM	[31]
Epoxy-graphite electrode	Electrochemical impedance spectroscopy	63.2 pM	50.0 pM to 50.0 nM	[32]
Graphene oxide /polyaniline/CdSe quantum dots	Electrogenerated chemiluminescence	20.0 nM	50.0 nM-100 μM	[33]
Carbon nanotubes/aptamer-antibody platform	Electrochemical impedance spectroscopy	12.0 pM	25.0 to 100 pM	[34]
Biotin-tagged aptamers /avidins / glass slide	Surface plasmon resonance	50.0 nM	80.0 pM to 80.0 nM	[35]
This work	Electrochemical impedance spectroscopy	1.66 pM	0.01 nM to 750 nM	-

Samples	CYC concentration	% Recovery	% RSD
Sample 1	100 nM	105	9.29
Sample 2	200 nM	101.5	11.2
Sample 3	300 nM	97.6	10.7

Table 2. Recovery studies performed in spiked serum samples for applicability of the proposed sensor (n = 5).

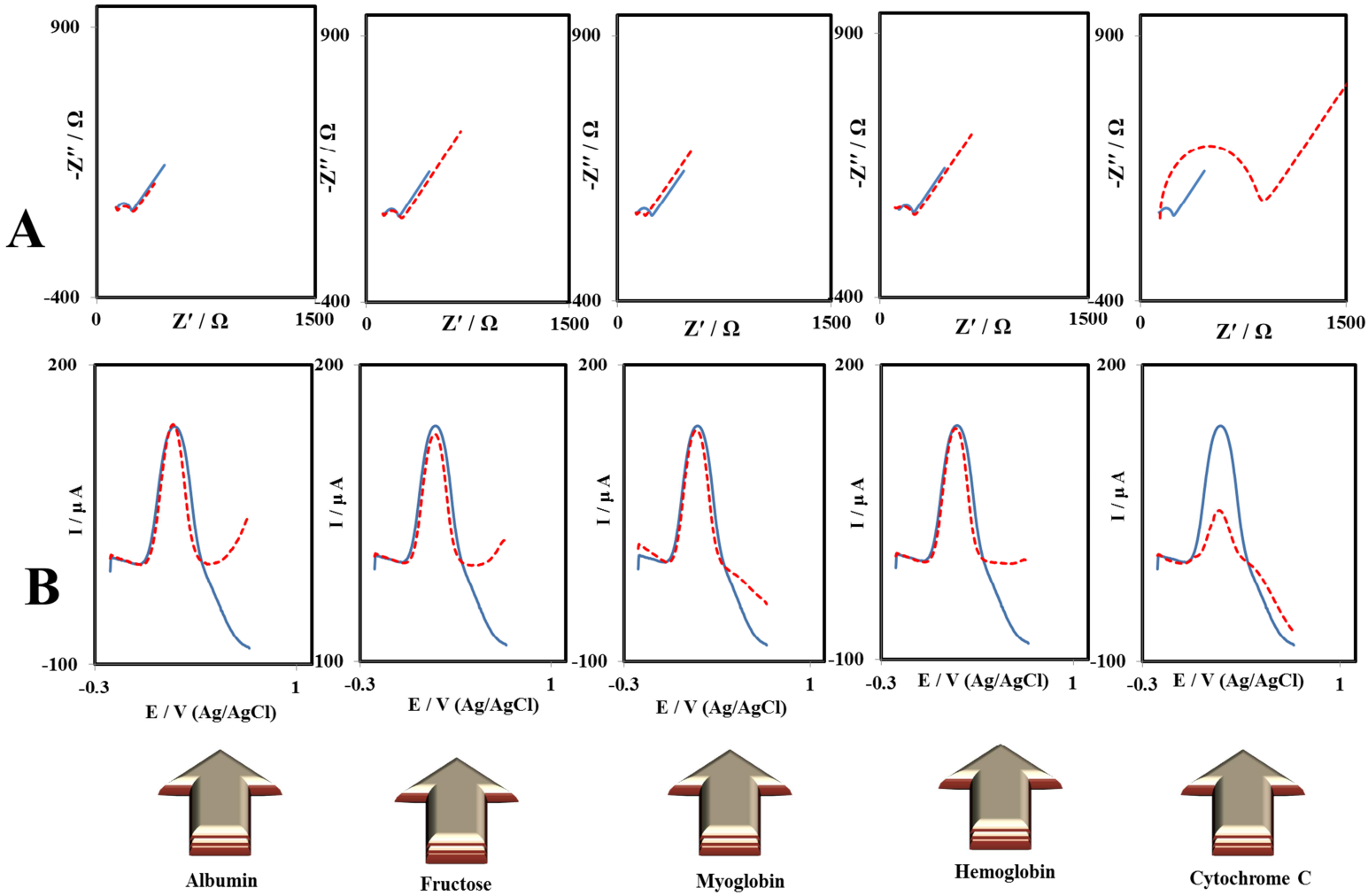
A
900
-400
-Z'' / Ω
0
Z' / Ω
1500
B
200
-100
I / μ A
-0.3
1
E / V (Ag/AgCl)
Albumin
Fructose
Myoglobin
Hemoglobin
Cytochrome C

Fig. 9

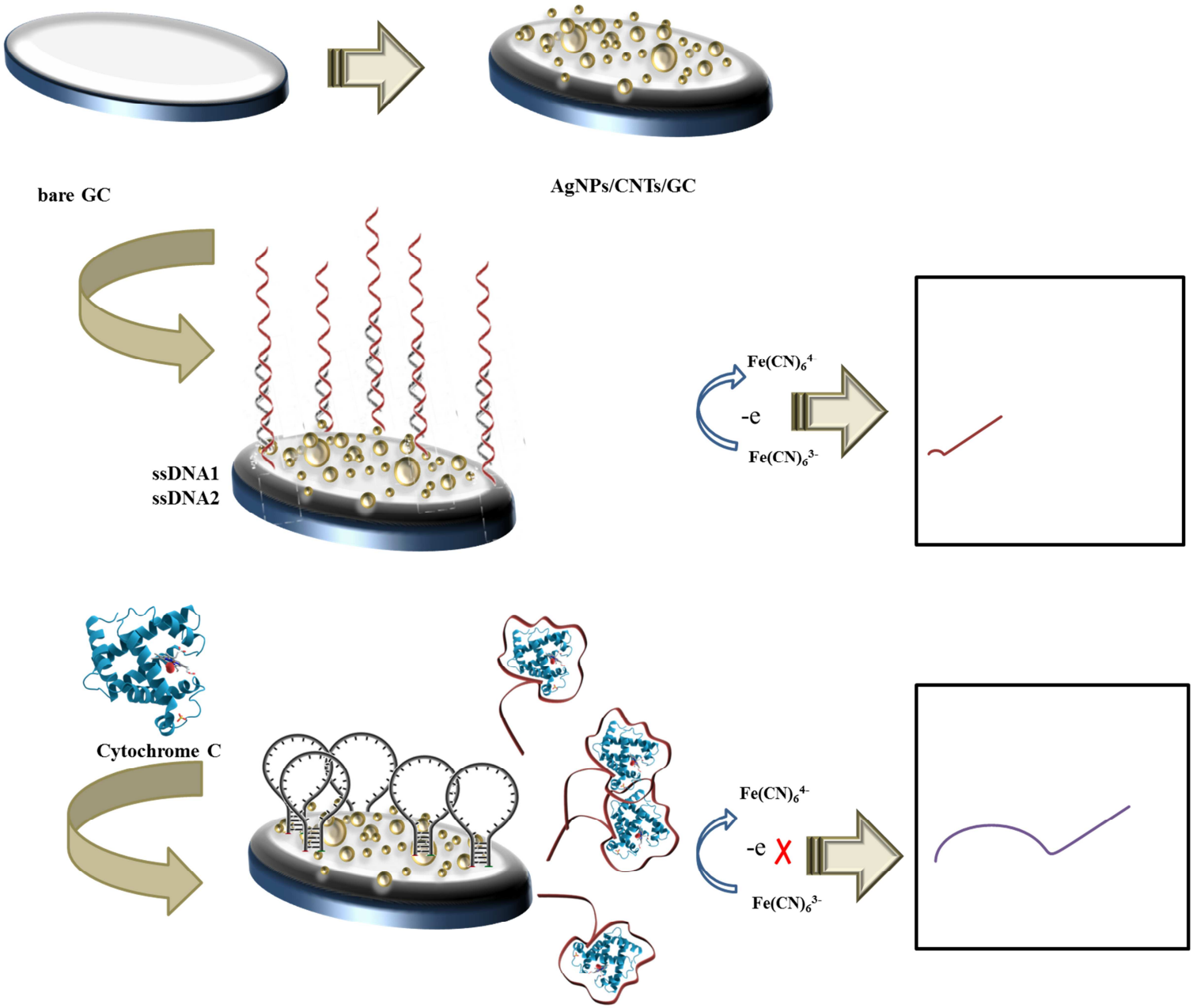
bare GC
AgNPs/CNTs/GC
ssDNA1
ssDNA2
$Fe(CN)_6^{4-}$
-e
$Fe(CN)_6^{3-}$
Cytochrome C
$Fe(CN)_6^{4-}$
-e
$Fe(CN)_6^{3-}$

Fig. 1

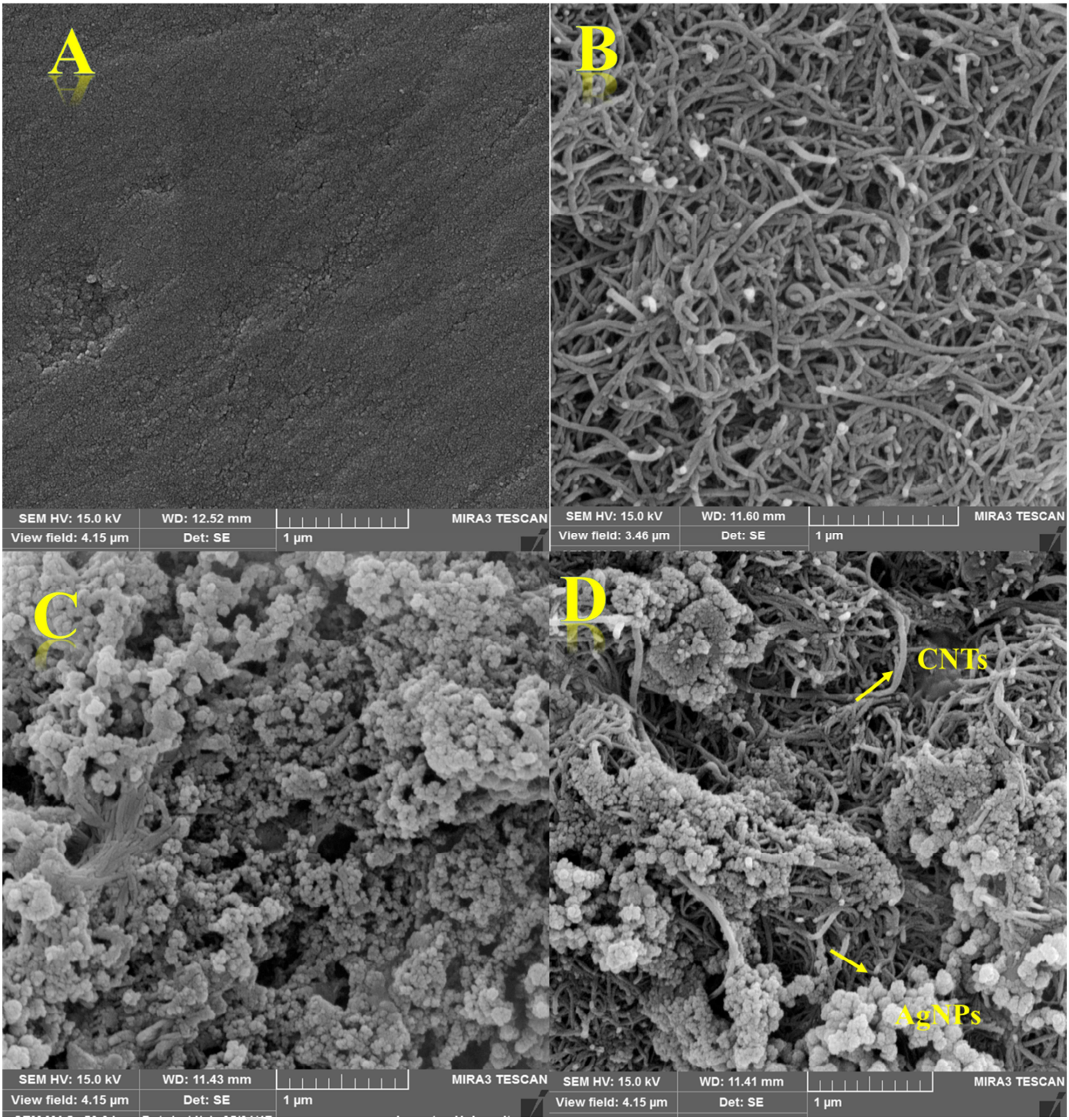
A
SEM HV: 15.0 kV
WD: 12.52 mm
MIRA3 TESCAN
View field: 4.15 μm
Det: SE
1 μm
B
SEM HV: 15.0 kV
WD: 11.60 mm
MIRA3 TESCAN
View field: 3.46 μm
Det: SE
1 μm
C
SEM HV: 15.0 kV
WD: 11.43 mm
MIRA3 TESCAN
View field: 4.15 μm
Det: SE
1 μm
D
CNTs
AgNPs
SEM HV: 15.0 kV
WD: 11.41 mm
MIRA3 TESCAN
View field: 4.15 μm
Det: SE
1 μm

Fig. 2

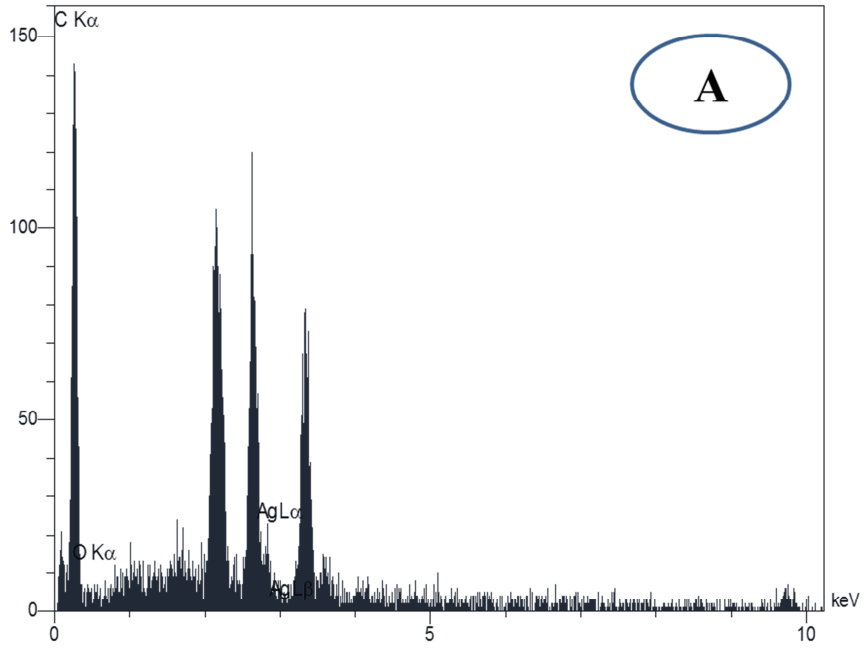

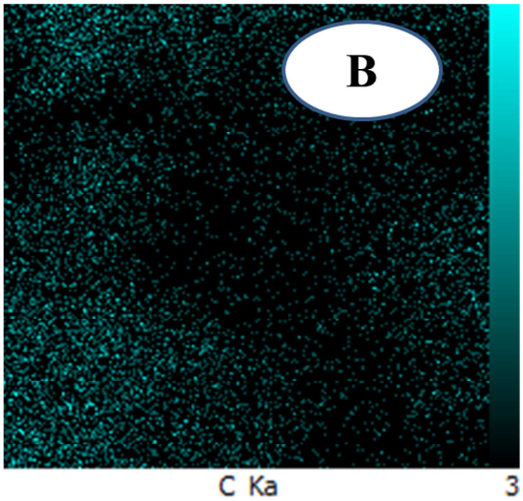

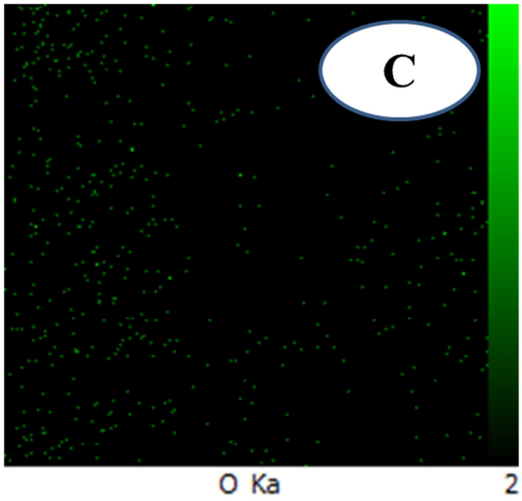

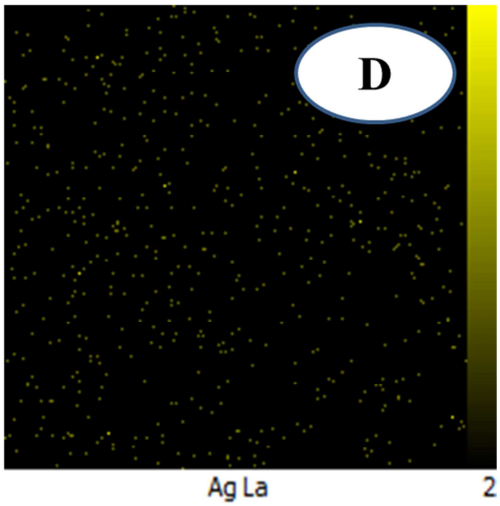

Fig. 3

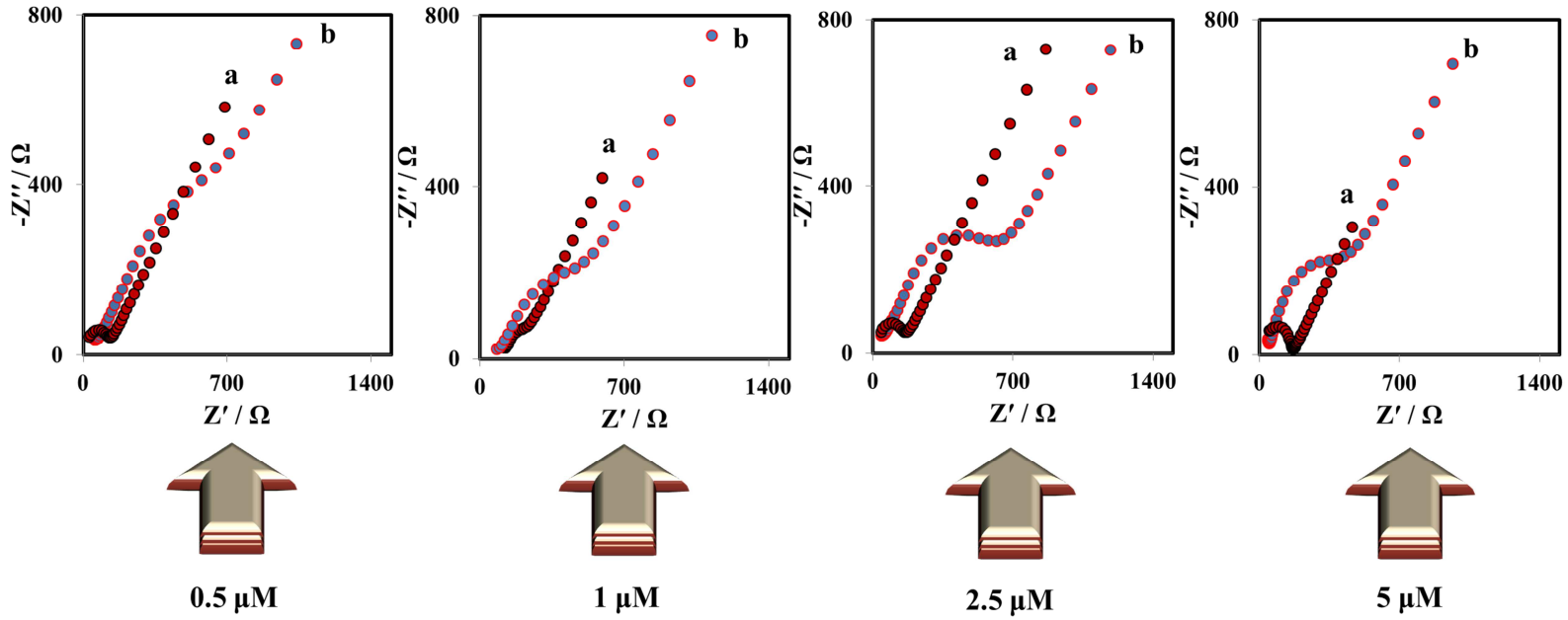

Fig. 4

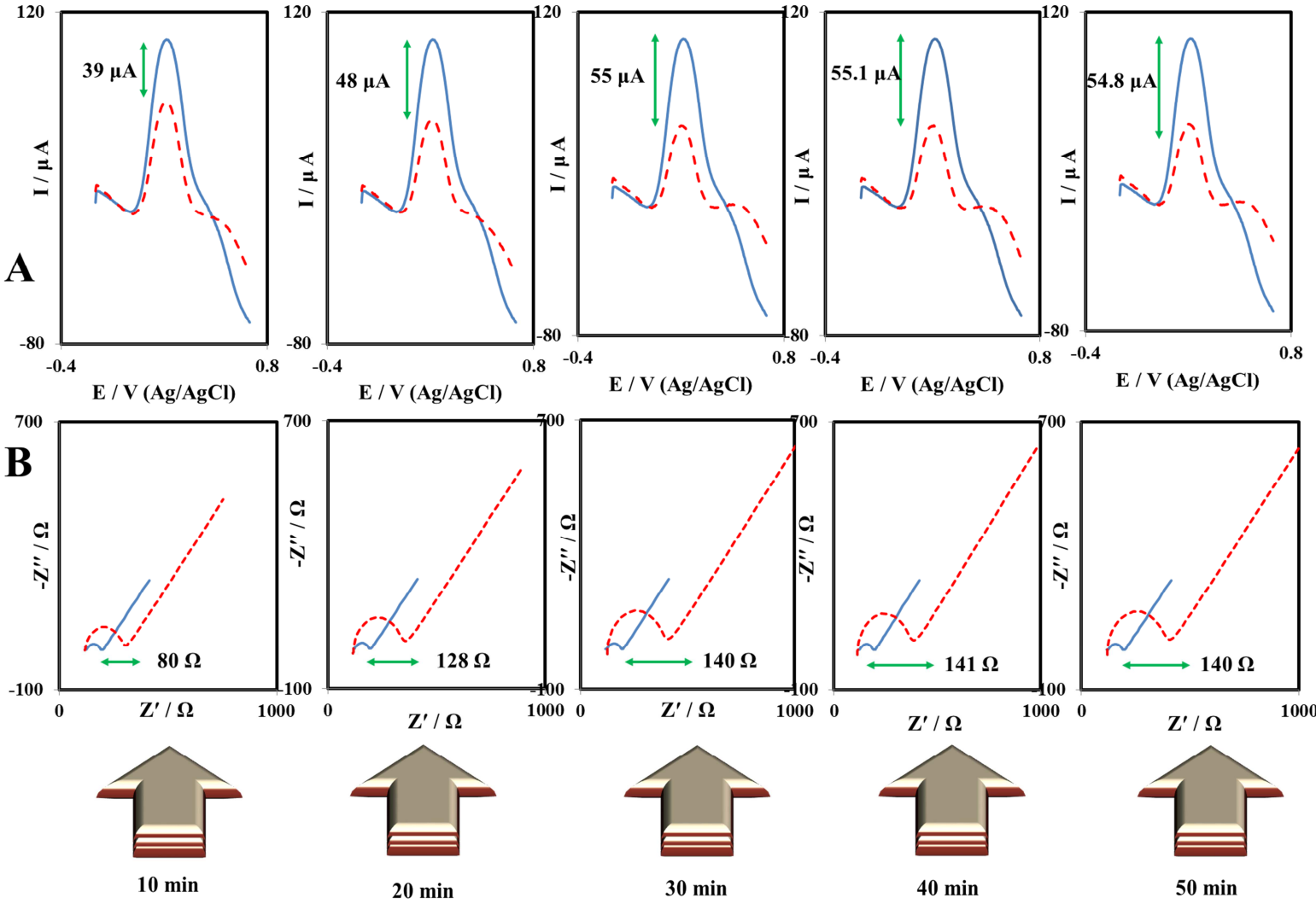

Fig. 5

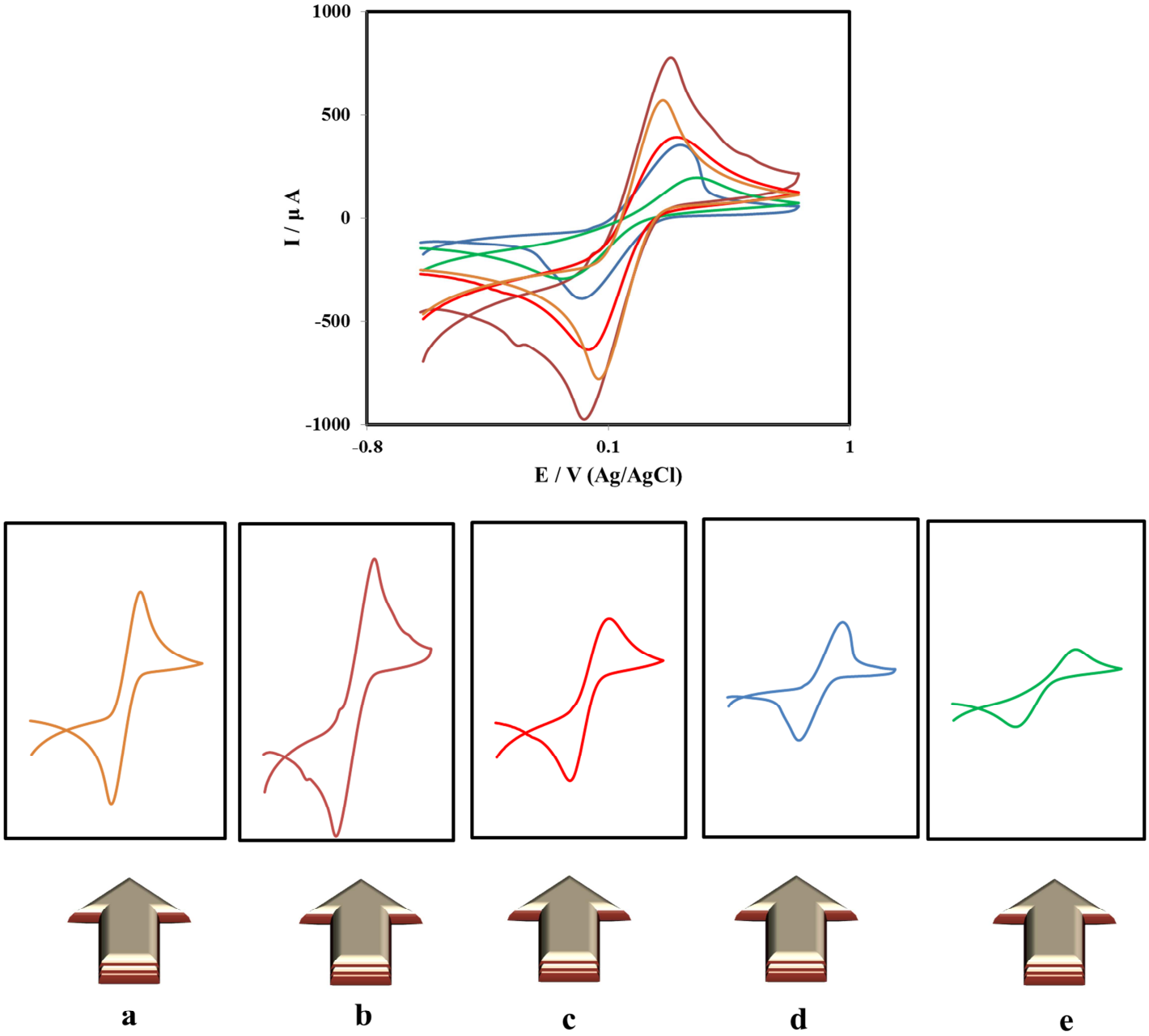

Fig. 6

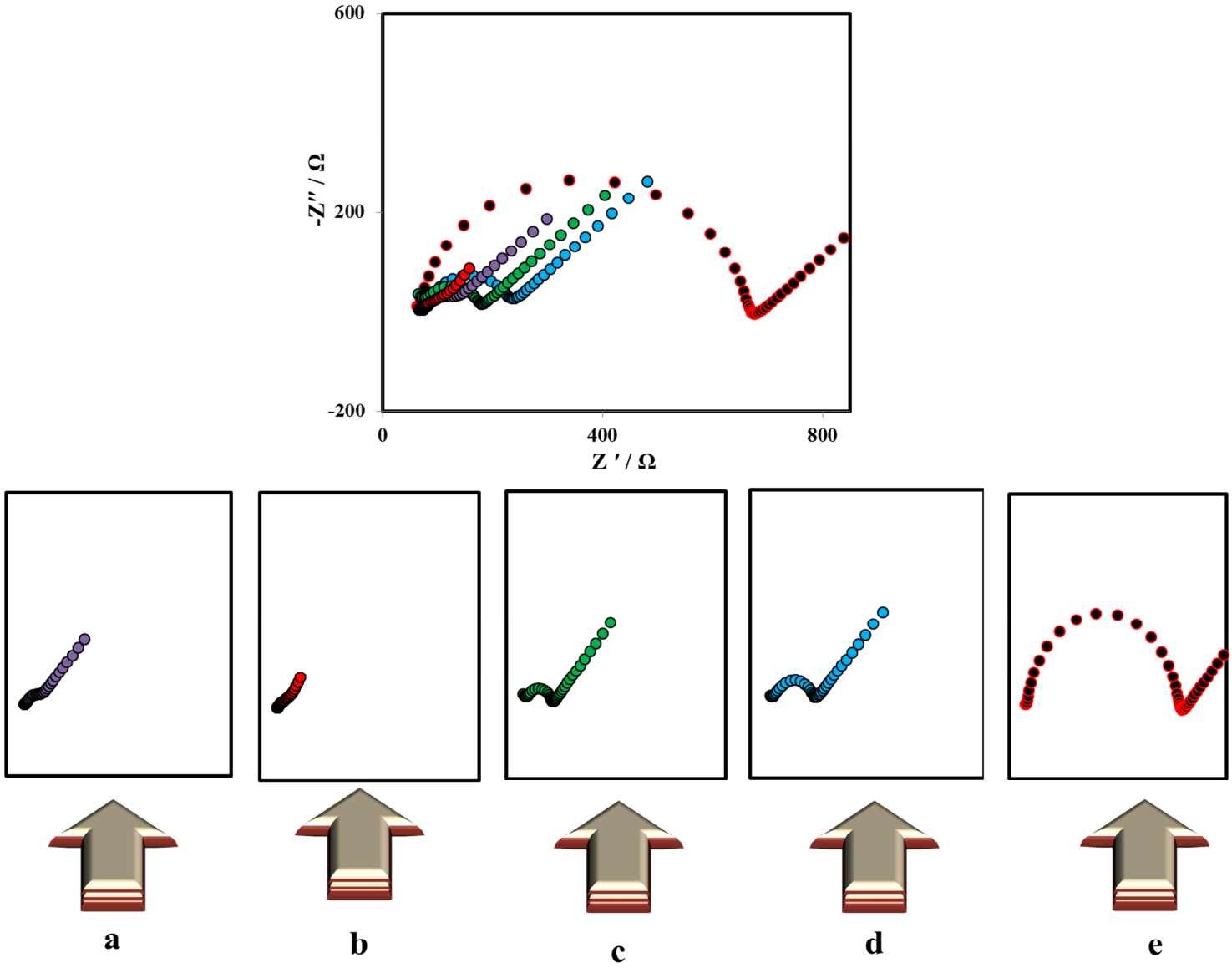

Fig. 7

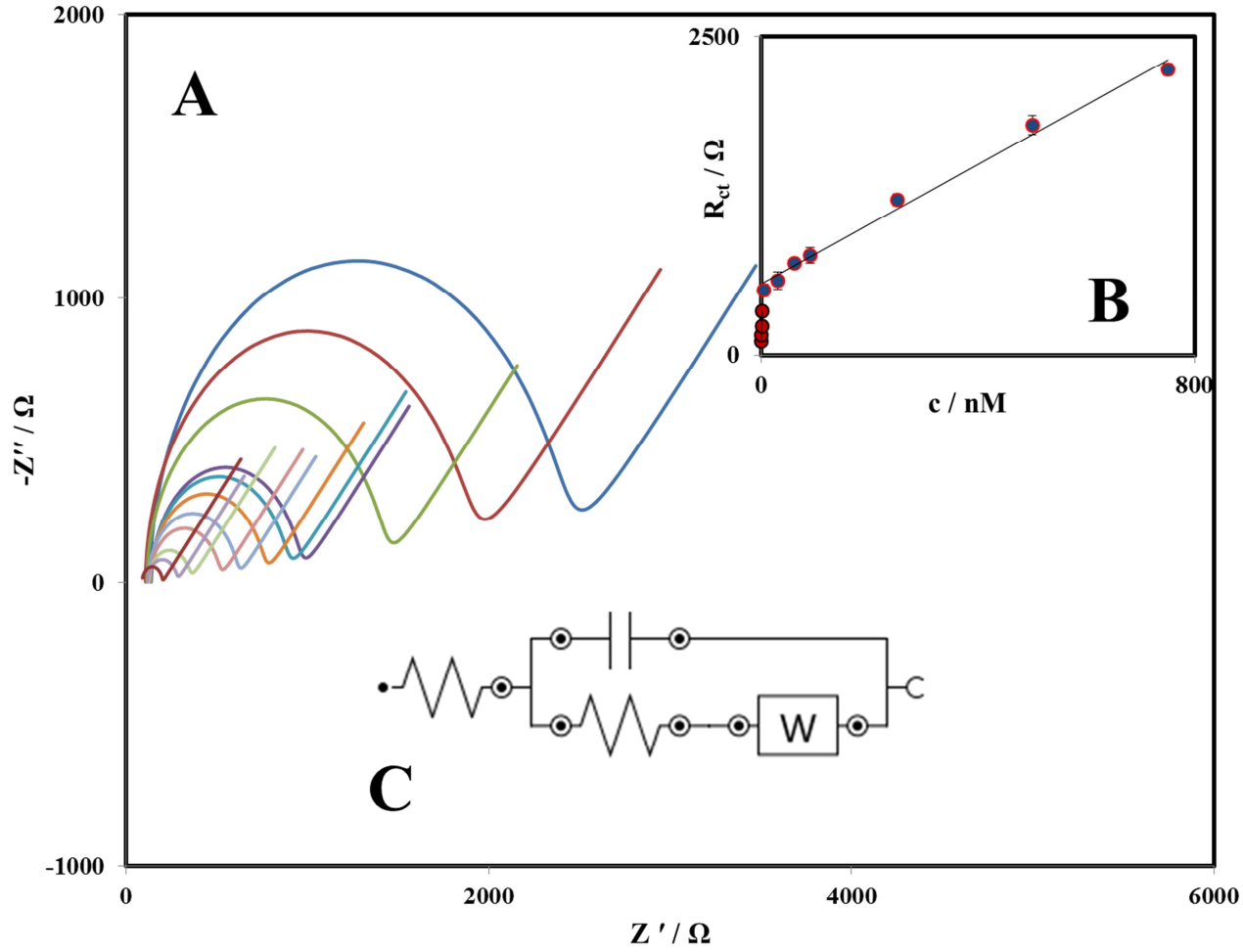

Fig. 8